PERGAMON

International Journal of Multiphase Flow 26 (2000) 635–661

International Journal of Multiphase Flow

www.elsevier.com/locate/ijmulflow

Heavy particle dispersion in inhomogeneous, anisotropic, turbulent flows

Xi-Qing Chen*

Department of Mechanical Engineering, University of Waterloo, Waterloo, Ont., Canada N2L 3G1

Received 7 May 1998; received in revised form 6 May 1999

Abstract

Detailed numerical studies were carried out using a hybrid Eulerian–Lagrangian model for heavy nickel particles dispersing in a turbulent gas flow. A second-moment closure model, based on curvilinear coordinates, was used for the prediction of the fluid flow field whereas an improved Lagrangian stochastic model was employed for the prediction of the particulate phase. The improved Lagrangian stochastic model has accounted for the turbulence inhomogeneity, turbulence anisotropy, and particle crossing-trajectories effect. In addition, the particle inertial effect that heavy particles may disperse more than fluid particles in the longtime limit was also taken into consideration based upon the recently published theoretic analysis. Numerical results were compared with available experimental measurements and with other numerical results for both the gas and particle phases. Various parametric studies, such as particle initial conditions, eddy time scale, eddy length scale, particle inertia and restitution coefficients were performed to understand how these parameters influenced numerical predictions. It was found that the present numerical results were generally in better agreement with the experimental measurements than those of the other modelers.

Keywords: Two-phase flows; Particle dispersion; Eddy-interaction model; Reynolds-stress model; Curvilinear coordinates

1. Introduction

Particle-laden turbulent flows are of great importance in many industrial applications, such

* Tel: +1 519 888 4567 x 5887 fax.: +519 888 6197.
E-mail address: x5chen@sunwise.uwaterloo.ca (X.-Q. Chen).

0301-9322/00/$ - see front matter
PII: S0301-9322(99)00049-X

as pneumatic transport of solids, pulverized coal combustion, classifiers and cyclones. To account for the effects of the particle-size spectrum, inter-particle collisions, particle-wall interaction, and crossing particle trajectories, the Lagrangian trajectory model has been widely used, in conjunction with the fluid-phase Eulerian formulation, to predict a variety of two-phase flows; see Shuen et al. (1985), Solomon et al. (1985) and Chen and Crowe (1984), among others. Among the Lagrangian trajectory models for particle turbulent dispersion, the particle-eddy interaction model of Gosman and Ioannides (1981), herein referred to as the GI model, has been widely applied to predict various particle-laden two-phase flows and spray flows with and without droplet evaporation; see Durst et al. (1984) and Chang and Wu (1994) and Chen and Pereira (1996). The current status of modeling two-phase flows has been reviewed by Crowe (1982) and Crowe et al. (1996), Sirignano (1993), and Elghobashi (1994), among others.

The conventional particle-eddy model assumes that a discrete heavy particle moving in a turbulent carrier flow encounters a series of turbulent energetic eddies randomly sampled from the carrier flow field. The particle is interacting with the eddy for a period of time, which is determined as the minimum of the eddy lifetime and the eddy transit time accounting for the crossing trajectory effect. Even though such an eddy interaction model has been widely applied with a great success to predict many dilute turbulent two-phase flows, the recent analyses (Graham, 1996a, 1996b; Graham and James, 1996) have shown that there exist some intrinsic model deficiencies. It was found that the original GI model could not account for the possibility that the finite-inertia particles may disperse faster than the fluid particles. This is due to the fact that the constraint imposed by the original GI model has led to the outcome that the finite-inertia particles can never interact with the eddy for a time longer than the fluid particles, thus underpredicting the dispersion of the finite-inertia particle in the longtime limit. Evidently, this is clearly in contrast to experimental observations that the finite-inertia particles may disperse more than the fluid particles. To take this physical phenomenon into account, Graham (1996a) proposed a modification on the original GI model by introducing an additional maximum particle-eddy interaction time scale, which is independent of the fluid particle interaction time (FPIT) scale. Given a turbulence structure parameter, the maximum time scale can be determined. Chen and Pereira (1998) found that such a modification improved their numerical predictions for the dispersion of glass beads with a mean diameter of 50 μm in a turbulent gas flow.

The original GI model for particle dispersion is based upon the Eulerian flow field predicted with the k–ε model. The local turbulent kinetic energy is used for sampling the eddy velocity fluctuations. Therefore, it cannot account for the turbulence anisotropy when anisotropically turbulent two-phase flows are considered. To account for the effect of the turbulence anisotropy on particle dispersion, Chen and Pereira (1995) found that the time-correlated particle dispersion model (Zhou and Leschziner, 1991) should be used. However, the time-correlated particle dispersion model increases the computational burden as compared to the original GI model. Later, Chen and Pereira (1996) found that the effect of turbulence anisotropy on particle dispersion could be accounted for by modifying the original GI model; using the local Reynolds stresses, instead of the local turbulent kinetic energy, to determine the eddy velocity fluctuations. It was shown that with this modification the anisotropic particle dispersion could be adequately predicted. In the original GI model, it is assumed that the eddy velocity fluctuations, sampled at the beginning of encounter, are kept unchanged until the end

of the particle-eddy interaction time. Evidently, this assumption results in an artificial transfer of turbulence from the region of high intensity to low intensity within an eddy interaction time. To overcome this drawback, MacInnes and Bracco (1992) suggested that the turbulence inhomogeneity could be accounted for by using a normalized fluctuating velocity at the beginning of encounter to define a physical scale. The local turbulence intensity is then used to determine the eddy fluctuating velocities at each time step.

The objective of the present work is to investigate the capability of an improved particle dispersion model to predict the dispersion of heavy nickel particles in a turbulent gaseous flow. Experimental measurements (Sato et al., 1996) are used to evaluate numerical predictions. The second-moment Reynolds-stress transport model is used for the carrier gas flow. The solution of the Reynolds-stress model is based on curvilinear coordinates, with an aim to generalize the feasibility of the present two-phase flow model to predict industrial two-phase flows with complex geometries, for example, the particle dispersion in an ultrasonic flow meter (Chen and Pereira, 1997). The improved particle-eddy interaction model can account for particle dispersion in inhomogeneous, anisotropic turbulent flows. Detailed numerical studies were carried out to clarify the influences of different parameters, such as eddy length and time scales, particle inertia, particle initial conditions and particle-wall interaction on two-phase flow predictions. In addition, the complete (momentum exchanges and turbulence modulation) and partial (only momentum exchanges) two-way coupling effects were also studied to isolate the contribution of the momentum exchanges from that of the turbulence modulation to the coupling effects. To evaluate the present two-phase flow model, numerical predictions were compared with both numerical and experimental results of Sato et al. (1996). In addition, the numerical results were also compared with those of Berlemont et al. (1997).

2. Reynolds-stress transport modeling of the continuous phase

For dilute two-phase flows, the particulate-phase concentration is typically less than 0.1%. As a result, the Eulerian governing equations for the continuous phase are similar to those for single-phase flows, except that the exchanges between the two phases are necessarily accounted for using a particle-source-in-cell model. For isothermal two-phase flows, two-phase exchanges occur in momentum equations. In addition, the turbulent modulation should also be considered in the equations of the turbulent kinetic energy and its dissipation rate. To cope with the possible geometric complexity encountered in many two-phase flows, the present Reynolds-transport equations are written and solved using Cartesian velocity vectors in curvilinear coordinates, the so-called partial transformation approach. In what follows, the Eulerian governing equations are briefly described. The time-averaged transport equations for continuity and momentum can be written tensorially in non-orthogonal curvilinear coordinates as:

$$\frac{\partial \rho U_m \beta_m^j}{\partial \xi_j} = 0 \tag{1}$$

$$\frac{\partial \rho U_m \beta_m^j U_i}{\partial \xi_j} = -\frac{\partial P}{\partial \xi_j}\beta_i^{\ j} + \frac{\partial}{\partial \xi_k}\left[-\rho \overline{u_i u_j}\beta_j^k \right] + S_{U_i}^{\mathrm{p}} \tag{2}$$

where the coefficient β's denote the cofactors of the co-ordinate transformations, J is the Jacobian determinant, P is the pressure, and $S_{U_i}^{\mathrm{p}}$ accounts for the two-phase momentum exchange. The Reynolds stresses are governed by

$$\frac{\partial \rho U_k \beta_k^m \overline{u_i u_j}}{\partial \xi_m} = \frac{\partial}{\partial \xi_n}\left[\frac{1}{J}\beta_k^n \rho C_{\mathrm{s}} \frac{k}{\varepsilon}\overline{u_k u_m}\beta_m^l \frac{\partial \overline{u_i u_j}}{\partial \xi_l} \right] + J\left[P_{ij} - \frac{2}{3}\rho\varepsilon\delta_{ij} + \phi_{ij} \right] + S_{ij}^{\mathrm{p}} \tag{3}$$

where P_{ij}, ϕ_{ij} and S_{ij}^{p} represent, respectively, the generation, pressure–strain processes, and two-way coupling sources between the continuous and particulate phases. The turbulent kinetic energy k is equal to $\frac{1}{2}\overline{u_i u_i}$. The exact generation term is given by

$$P_{ij} = -\rho\left[\overline{u_j u_k}\frac{1}{J}\frac{\partial U_i}{\partial \xi_m}\beta_k^m + \overline{u_i u_k}\frac{1}{J}\frac{\partial U_j}{\partial \xi_n}\beta_k^n \right] \tag{4}$$

The pressure–strain terms are modeled using the proposal of Gibson and Launder (1978):

$$\phi_{ij} = \phi_{ij,1} + \phi_{ij,2} + \phi_{ij,1}^{\mathrm{w}} + \phi_{ij,2}^{\mathrm{w}} \tag{5}$$

where the first and second terms on the right-hand side denote the 'return-to-isotropy' and the 'rapid' contribution, respectively. The remaining two terms are the corresponding corrections to account for the effects of wall-induced pressure reflections. Each term in Eq. (5) is given as follows:

$$\phi_{ij,1} = -C_1\rho\frac{\varepsilon}{k}\left[\overline{u_i u_j} - \frac{2}{3}k\delta_{ij} \right], \quad \phi_{ij,2} = -C_2\left[P_{ij} - \frac{1}{3}P_{kk}\delta_{ij} \right] \tag{6}$$

$$\phi_{ij,1}^{\mathrm{w}} = C_1'\rho\frac{\varepsilon}{k}\left[\overline{u_l u_m}n_l n_m\delta_{ij} - \frac{3}{2}\overline{u_l u_i}n_l n_j - \frac{3}{2}\overline{u_l u_j}n_l n_i \right] f \tag{7}$$

$$\phi_{ij,2}^{\mathrm{w}} = C_2'\left[\phi_{lm,2}n_l n_m\delta_{ij} - \frac{3}{2}\phi_{il,2}n_l n_j - \frac{3}{2}\phi_{jl,2}n_l n_i \right] f \tag{8}$$

where n_i denotes the ith component of a unit vector normal to the wall, and f is the function of the wall-oriented distance, Δx_n, given by

$$f = \frac{k^{3/2}/\varepsilon}{2.45\Delta x_n} \tag{9}$$

The dissipation rate of the turbulent kinetic energy, ε, is governed by

$$\frac{\partial \rho \beta_k^m U_k \varepsilon}{\partial \xi_m} = \frac{\partial}{\partial \xi_n}\left[\frac{1}{J}\beta_k^n \rho C_\varepsilon \frac{k}{\varepsilon}\overline{u_k u_m}\beta_m^l \frac{\partial \varepsilon}{\partial \xi_l} \right] + J\frac{\varepsilon}{k}[C_{\varepsilon 1}G - C_{\varepsilon 2}\rho\varepsilon] + C_{\mathrm{p}\varepsilon}\rho\frac{\varepsilon}{2k}S_{mm}^{\mathrm{p}} \tag{10}$$

where the last term S_{mm}^{p} accounts for the turbulence modulation by the dispersed phase. The

production term of the turbulent kinetic energy is given by $G = 0.5P_{kk}$. The model constant $C_{p\varepsilon}$ has a value ranging from 1.1 to 2.0. The value of 1.6 was chosen for the present two-phase flow, as suggested by Sato et al. (1996), to have the same turbulence attenuation as the experiment. Table 1 lists all the model constants used in Eqs. (3)–(10).

3. Stochastic-trajectory modeling of the particulate phase

Discrete heavy particles are moving in turbulent carrier flows based on the Lagrangian trajectory equations. Each Lagrangian trajectory is representative of a 'parcel' of particles having the same velocity and initial conditions. Therefore, each individual particle trajectory has its own representative number flow rate. The total number of particle trajectories conserves the mass flow rate at the inlet. Since the density ratio of the gas to nickel particles is very small, the main forces acting on a particle are the drag and gravity. All other forces, such as the lift and Basset forces can be neglected. The final particle trajectory equation can be written as

$$\frac{\mathrm{d}\tilde{U}_{\mathrm{p}i}}{\mathrm{d}t} = \frac{\tilde{U}_i - \tilde{U}_{\mathrm{p}i}}{\tau_{\mathrm{p}}} f_{\mathrm{p}} + g_i \tag{11}$$

where $\tilde{U}_i$ denotes the instantaneous velocity of the carrier fluid following the motion of the heavy particle, f_{p} the drag correction coefficient, and g_i the gravitational force. Obviously, the mean part of the instantaneous velocity can be obtained using an approach to interpolate the Eulerian fluid property to the heavy particle position, whereas the fluctuating part is not available with the time-averaged Eulerian equations. It is aimed at modeling this fluctuating part that many Lagrangian stochastic models have been developed (Gosman and Ionnides, 1981; Berlemont et al., 1990; Zhou and Leschziner, 1991). However, the most popular and frequently used particle-dispersion model should be the one of Gosman and Ioannides (1981). Details on this model and its improvements will be given later after the two-way coupling sources. Particle positions in the computational domain are updated each time step by

$$\frac{\mathrm{d}x_i}{\mathrm{d}t} = \tilde{U}_{\mathrm{p}i} \tag{12}$$

which can be integrated after obtaining the particle velocity. In addition, the two-phase coupling sources can be determined as follows.

Even though dilute two-phase flows can neglect the effect of the particulate-phase concentration on the Eulerian equations, it is still necessary to account for coupling effects of momentum exchanges and turbulence modulation. This is because the particle density is often

Table 1
Reynolds-stress model constants

C_s	C_ε	C_1	C_2	C_1'	C_2'	$C_{\varepsilon 1}$	$C_{\varepsilon 2}$	$C_{p\varepsilon}$
0.22	0.18	1.8	0.6	0.5	0.3	1.45	1.9	1.6

much larger than the continuous phase. The momentum exchanges between the continuous and particulate phases can be determined as (Durst et al., 1984)

$$S^{\mathrm{p}}_{U_i} = \frac{1}{\forall}\sum \dot{N}_k\left[\Delta\tilde{U}_{\mathrm{p}i} - g_i\Delta t\right]\frac{\pi}{6}\rho_{\mathrm{p}}D^3_{\mathrm{p}} \tag{13}$$

where $\forall$ is a Eulerian control volume, $\Delta\tilde{U}_{\mathrm{p}i}$ the velocity change of the particle residing in the control volume $\forall$ for a time interval Δt, $\dot{N}_k$ the number flow rate of the kth particle, and D_{p} the particle diameter, the summation made over all particle trajectories across the control volume $\forall$. The exchanges in Reynolds stresses are taken into account by including (Kohnen and Sommerfeld, 1997) in the Eulerian equations a source term as follows:

$$S^{\mathrm{p}}_{ij} = \langle\tilde{U}_i\tilde{S}^{\mathrm{p}}_{U_j}\rangle - \langle\tilde{U}_j\rangle\langle\tilde{S}^{\mathrm{p}}_{U_i}\rangle + \langle\tilde{U}_j\tilde{S}^{\mathrm{p}}_{U_i}\rangle - \langle\tilde{U}_i\rangle\langle\tilde{S}^{\mathrm{p}}_{U_j}\rangle \tag{14}$$

where $\tilde{S}^{\mathrm{p}}_{U_i} = -\frac{1}{\forall}\dot{N}_k[\Delta\tilde{U}_{\mathrm{p}i} - g_i\Delta t]\frac{\pi}{6}\rho_{\mathrm{p}}D^3_{\mathrm{p}}$. Note that here $\langle\ \rangle$ denotes an ensemble average for all the particle trajectories crossing the control volume. Consequently, the extra turbulence dissipation in the ε-equation can be determined.

4. Improved particle-eddy interaction model

Since its development, the particle-eddy interaction model of Gosman and Ioannides (1981), referred to as the GI model, has been subjected to many improvements; see Shuen et al. (1985), Chen and Pereira (1995), Graham and James (1996), Graham (1996a, 1996b), among others. The original particle-eddy interaction model assumes that a particle moving in a turbulent carrier flow will encounter a series of energetic eddies. Each eddy is characterized by a turbulent time scale and a turbulent length scale. The particle is interacting with a randomly sampled eddy for a period of time, which is the minimum of an eddy lifetime and an eddy transit time. The eddy transit time is aimed at accounting for the particle trajectory crossing effect, which usually reduces particle dispersion.

Following Gosman and Ioannides (1981), the time and length scales for an energetic eddy are determined as follows:

$$t_{\mathrm{e}} = \sqrt{\frac{3}{2}}C_\mu^{3/4}\frac{k}{\varepsilon}, \quad l_{\mathrm{e}} = C_\mu^{3/4}\frac{k^{3/2}}{\varepsilon} \tag{15}$$

where C_μ is the model constant equal to 0.09. Since heavy particles may cross an eddy due to the relative motion, this will reduce the particle dispersion. An eddy transit time scale is introduced as a result. Neglecting the influence of the gravity, we may obtain the eddy transit time using the linearized particle momentum equation as follows:

$$t_{\mathrm{c}} = -\tau^*_{\mathrm{p}}\ln\left[1 - \frac{l_{\mathrm{e}}}{V_{\mathrm{rel}}\tau^*_{\mathrm{p}}}\right] \tag{16}$$

where V_{rel} is the relative velocity between the two phases and τ^*_{p} is the particle relaxation time, given by

$$\tau_p^* = \frac{\tau_p}{f_p} \tag{17}$$

with τ_p being the particle relaxation time. The particle-eddy interaction time for the GI model is, therefore, determined by

$$t_{int} = \begin{cases} T_f = t_e & \text{if } V_{rel} < \dfrac{l_e}{\tau_p^*} \\ \min(t_e, t_c) & \text{otherwise} \end{cases} \tag{18}$$

where T_f denotes the fluid particle interaction time (FPIT), as called by Graham (1996a, 1996b). It is clear that the original GI model simply states that the eddy interaction time for heavy particles cannot exceed the fluid particle interaction time, T_f. As a consequence, the heavy particle dispersion can never exceed the fluid particle dispersion.

4.1. Effect of turbulence anisotropy

One of the shortcomings for applying the original GI model to anisotropic turbulent two-phase flows is that it uses the local turbulent kinetic energy to determine the sampled eddy velocity fluctuations. This is acceptable when the k–ε model is used for simulating the turbulent fluid flow. This is due to the fact that no reliable information on turbulence anisotropy has been obtained with the k–ε model. The outcome of using the local turbulent kinetic energy for sampling the eddy fluctuating velocities is that the particle dispersion will also become isotropic, and that the turbulence anisotropy of the particulate phase will not be adequately predicted (Chen and Pereira, 1995). It is, therefore, suggested (Chen and Pereira, 1995) that the local Reynolds stresses be used for sampling the eddy fluctuating velocities. The eddy velocity fluctuation at the beginning of encounter is sampled by

$$u_i = \left(\overline{u_i^2}\right)^{1/2} \zeta \text{ (no summation over subscript } i) \tag{19}$$

where $(\overline{u_i^2})^{1/2}$ is the normal stress of the gas flow, and ζ is the random Gaussian variable having zero mean and unity deviation. The Reynolds stresses in Eq. (19) can be obtained using any numerical algorithm to interpolate the Eulerian solution to the heavy particle position.

4.2. Effect of turbulence inhomogeneity

Even though the original GI model has been modified to account for turbulence anisotropy, it still has the drawback that it does not account for turbulence inhomogeneity for inhomogeneous turbulent two-phase flows. The original GI model assumes that the fluctuating velocities sampled for an eddy are kept unchanged for the period of time during which the particle is interacting with the sampled eddy. Evidently, this will result in an artificial transfer of fluid turbulence from the region of high intensity to low intensity (MacInnes and Bracco, 1992). To overcome this deficiency, it is, therefore, assumed that the particle is always influenced by the local turbulence. The normalized fluctuating velocities that are obtained at the beginning of a particle-eddy encounter are multiplied by the local turbulence intensity,

obtained with the second-moment closure model. In this way, the effect of fluid turbulence inhomogeneity on particle dispersion can be accounted for.

4.3. Effect of particle inertia

The recent theoretical studies of the GI model (Graham and James, 1996, Graham, 1996a, 1996b) have demonstrated that the original GI model has the deficiency of underpredicting the heavy particle dispersion in the longtime limit as compared to the tracer particles. This is due to the constraint used within the conventional GI model that non-fluid particles interact with a given eddy for a time less than the eddy lifetime. However, experimental measurements indicate that heavy particles may disperse faster than tracer particles in the longtime limit. Following Graham (1996a), this deficiency has been overcome by modifying the way to determine the particle-eddy interaction time t_{int} as follows:

$$t_{\text{int}} = \begin{cases} T_{\text{f}} = 2t_{\text{e}} & \text{if } V_{\text{rel}} < \dfrac{2l_{\text{e}}}{\tau_{\text{p}}^*} \\ \min(T_{\max}, t_{\text{c}}) & \text{otherwise} \end{cases} \tag{20}$$

where t_{c} is given by Eq. (16), but l_{e} is doubled, as suggested by Graham (1996a, 1996b). The eddy lifetime t_{e} is multiplied by a factor of 2 for the FPIT to ensure that the Lagrangian integral time scales of the actual and model turbulence are consistent. Similarly, the multiplying factor of 2 for the eddy length scale is aimed at ensuring that the longitudinal scales of the actual and model turbulence are equal. The maximum interaction time $T_{\max}$ is independent of the fluid particle interaction time T_{f}. The introduction of $T_{\max}$ makes it possible for heavy particles to interact more time than the fluid particles with a sampled eddy. In such a way, heavy particles can disperse more than fluid particles in the long-time limit. Given a turbulence structure parameter, $T_{\max}$ can be set to some value to achieve a desired ratio of the Lagrangian to Eulerian time scales. Following Graham (1996a), it can be determined, using his Fig. 2, for a turbulence structure parameter equal to 1, $T_{\max} = 3.16t_{\text{e}}$ for a ratio of the Lagrangian to Eulerian time scales equal to 1.4. Setting $T_{\max} = T_{\text{f}} = t_{\text{e}}$, we can retrieve the original GI model.

5. Particle-wall impact model

When heavy particles rebound from the wall, some energy will be lost as a result of particle-wall interaction. It is, therefore, necessary to model the particle-wall interaction. The particle-wall interaction is a complex phenomenon. It may require accounting for the non-sphericity of particle shape (Gavze and Shapiro, 1997), for example. Evidently, the profound investigation of particle-wall interaction models is beyond the scope of the present work; therefore, a simple particle-wall impact model (Jun and Tabakoff, 1994) is applied here. This model uses the particle-wall impact angle to determine the restitution coefficients after rebounding from the wall; see Fig. 1. The unit normal and tangential vectors are denoted by $\vec{n}$ and $\vec{t}$, respectively. Let $\vec{V}_n$ be the decomposition of the particle velocity vector, $\vec{V}_{\text{p}}$, in the normal direction. The

tangential component can thus be determined by

$$\vec{V}_t = \vec{V}_\mathrm{p} - \vec{V}_n \tag{21}$$

The particle velocity after it rebounds from the wall can be determined by

$$\vec{V}_n' = -e_n \vec{V}_n, \quad \vec{V}_t' = e_t \vec{V}_t \tag{22}$$

where e_t and e_n are two restitution coefficients in the normal and tangential directions, respectively. It follows that the particle velocity after interacting with the wall is given by

$$\vec{V}_\mathrm{p}' = e_t \vec{V}_\mathrm{p} - (e_n + e_t)\vec{V}_n \tag{23}$$

from which each component of the particle velocity vector after rebounding from the wall can be determined. In accordance with Jun and Tabakoff (1994), the restitution coefficients can be determined in terms of the particle impact angle (β) as follows:

$$e_t = 1 - 2.12\beta + 3.0775\beta^2 - 1.1\beta^3, \quad e_n = 1 - 0.4159\beta + 0.4994\beta^2 - 0.292\beta^3 \tag{24}$$

where the impact angle is in radian, and is defined in Fig. 1. It was found that the impact angles were very small for the present nickel particles.

6. Boundary conditions and description of the two-phase flow

In the present work, one of the experimental cases of Sato et al. (1996) was considered. The experimental case was concerned with heavy nickel particles, having a density of 8404 kg/m^3, a mean diameter of 50.3 μm and a standard diameter deviation of 6.68 μm, dispersing in a turbulent gas flow. This flow case was selected for the present work because of the small density ratio of the gas to heavy nickel particles, which makes it possible to neglect all other forces but the drag and gravity. The heavy particles were injected from a near-wall jet having a

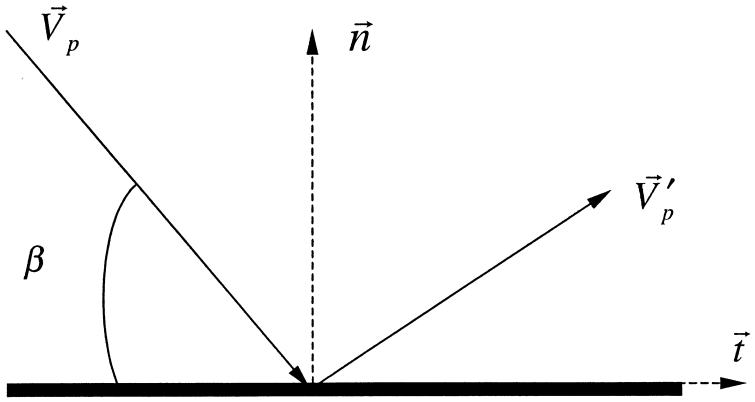

Fig. 1. Definition of the particle impact angle.

jet width of $b = 5$ mm. At the inlet, the fluid mean velocity was about 10 m/s, whereas the nickel particles had a mean axial velocity of about 5.6 m/s. Away from the near-wall jet, the uniform free-stream gas velocity was 2 m/s. Experimental measurements were available for both the gas and particle phases starting from $x/b = 1$. Therefore, numerical computations also started there. The flow domain for numerical computations consisted of 500×100 mm along the x- and y-directions, respectively. The gravitational acceleration was aligned with the x-direction. The computational domain was covered with 120×91 non-orthogonal grids, which gave an almost grid-independent solution for the fluid flow. The solution to the Reynolds-stress equations in curvilinear coordinates requires paying particular attention to implementing boundary conditions. In addition, the technique of introducing the artificial viscosity (Lien and Leschziner, 1996) is also necessary to enhance numerical stability. In the near-wall region, the conventional wall-function method was applied to modify the momentum equations. As discussed before (Chen and Pereira, 1998), such wall modifications for single-phase flows can still be used for a turbulent dilute two-phase flow, where the particle volume concentration is typically smaller than 0.05% (Rizk and Elghobashi, 1989). The boundary conditions for the Reynolds stresses were based on the practice of using fixed values for the wall-adjacent nodes (Lien and Leschziner, 1994). At the exit, the zero-gradient conditions were set for all the variables. The convergence criterion for the two-phase flow computations was set equal to 0.5% for all the normalized residuals after including two-way coupling sources. The initial distribution of particle sizes was selected by summing over the mean diameter a random part that obeys a Gaussian distribution. Similarly, the particle instantaneous velocities were sampled from the measured mean and root-mean-squared (RMS) values. To achieve a stochastically invariant solution, a total of 20,000 particle trajectories were tracked for the modified Lagrangian stochastic model. Of particular note is that the tracking of particles in non-orthogonal numerical grids requires an efficient numerical algorithm (Chen, 1997) to locate the Eulerian control volume to which the particle has moved after each Lagrangian time step. In the present work, a new particle-locating approach (Chen and Pereira, 1999) was used that can simultaneously locate the particle and distribute coupling sources over the particle trajectory-crossed Eulerian control volumes.

7. Results and discussion

To clarify the effect of different factors on numerical predictions, several numerical runs were performed in the present study. The numbering of runs and parametric descriptions are listed in Table 2.

Note that Runs 1–3 were aimed at clarifying the influence of time and length scales, as well as particle inertia on numerical results. Run 3 has accounted for the correct time and length scales, as well as the effect of particle inertia, proposed by Graham (1996a). Therefore, this run will be regarded as the standard one for comparison. Runs 4–6 were focused on understanding the effect of the initial particle mean transverse velocity on numerical predictions, especially the particle volume concentration. The effects of the particle-wall interaction on predictions were studied in terms of Runs 7–9. The coupling effects on two-phase flow predictions were investigated in terms of Runs 3, 10 and 11. These runs can clarify how the complete two-way

Table 2
Run labels and parametric descriptions

Run nos.	FPIT	Eddy length scale	Inertia effects	Restitution coefficients	Inlet velocity	Two-phase couplings
1	$T_f = t_e$	l_e	$T_{max} = t_e$	$e_t = 1.0$, $e_n = 1.0$	$\tilde{V}_p = V_{exp} + v_{exp}\zeta$	Momentum and turbulence
2	$T_f = 2t_e$	$2l_e$	$T_{max} = 2t_e$	$e_t = 1.0$, $e_n = 1.0$	$\tilde{V}_p = V_{exp} + v_{exp}\zeta$	Momentum and turbulence
3	$T_f = 2t_e$	$2l_e$	$T_{max} = 3.16t_e$	$e_t = 1.0$, $e_n = 1.0$	$\tilde{V}_p = V_{exp} + v_{exp}\zeta$	Momentum and turbulence
4	$T_f = 2t_e$	$2l_e$	$T_{max} = 3.16t_e$	$e_t = 1.0$, $e_n = 1.0$	$\tilde{V}_p = 0.5V_{exp} + v_{exp}\zeta$	Momentum and turbulence
5	$T_f = 2t_e$	$2l_e$	$T_{max} = 3.16t_e$	$e_t = 1.0$, $e_n = 1.0$	$\tilde{V}_p = 0.25V_{exp} + v_{exp}\zeta$	Momentum and turbulence
6	$T_f = 2t_e$	$2l_e$	$T_{max} = 3.16t_e$	$e_t = 1.0$, $e_n = 1.0$	$\tilde{V}_p = v_{exp}\zeta$	Momentum and turbulence
7	$T_f = 2t_e$	$2l_e$	$T_{max} = 3.16t_e$	Jun and Tabakoff (1994)	$\tilde{V}_p = V_{exp} + v_{exp}\zeta$	Momentum and turbulence
8	$T_f = 2t_e$	$2l_e$	$T_{max} = 3.16t_e$	$e_t = 0.9$, $e_n = 0.8$	$\tilde{V}_p = V_{exp} + v_{exp}\zeta$	Momentum and turbulence
9	$T_f = 2t_e$	$2l_e$	$T_{max} = 3.16t_e$	$e_t = 0.9$, $e_n = 0.6$	$\tilde{V}_p = V_{exp} + v_{exp}\zeta$	Momentum and turbulence
10	$T_f = 2t_e$	$2l_e$	$T_{max} = 3.16t_e$	$e_t = 1.0$, $e_n = 1.0$	$\tilde{V}_p = V_{exp} + v_{exp}\zeta$	Only momentum coupled
11	$T_f = 2t_e$	$2l_e$	$T_{max} = 3.16t_e$	$e_t = 1.0$, $e_n = 1.0$	$\tilde{V}_p = V_{exp} + v_{exp}\zeta$	No coupling sources

coupling (momentum and turbulence modulation), the partial two-way coupling (only momentum) and one-way coupling influence two-phase flow predictions. It should be noted that, due to too many runs performed here, only the most representative results are presented below.

7.1. Model evaluation with measurements and other numerical results

An accurate prediction of the single-phase flow field is a prerequisite for an accurate prediction of coupled two-phase flows. To evaluate the capability of the present two-phase flow model, therefore, the numerical results are first necessarily evaluated for the single-phase gas flow. To assess the present Reynolds-stress model, the numerical predictions are compared with both the experimental measurements and the numerical results of Sato et al. (1996). In addition, some available numerical results of Berlemont et al. (1997) are also compared here. Fig. 2(a)–(c) show the predicted and measured profiles of the gas axial mean velocity, the gas axial and transverse RMS velocities, respectively, at station $x = 200$ mm. Fig. 2(a) shows that slightly better near-wall predictions of the gas axial mean velocity are obtained with the low-Reynolds number k–ε model used by Sato et al. (1996). Such a near-wall improvement in the predicted gas axial mean velocity is probably attributed to the modification of some model coefficients in the low-Reynolds number k–ε model to account for the effect of wall approximation. The predictions of the present Reynolds-stress model lie between the low-Reynolds number k–ε model used by Sato et al. (1996) and the standard k–ε model used by Berlemont et al. (1997). Further away from the wall, the predictions with the Reynolds-stress model are in better agreement with the measurements of Sato et al. (1996), showing the superiority of the Reynolds-stress model to the two versions of the k–ε models.

The gas fluctuating velocities, shown in Fig. 2(b) and (c), obtained with the three models show that the Reynolds-stress model can capture the turbulence anisotropy, even though it overpredicts the gas axial RMS velocity. On the contrary, the two versions of the k–ε models used by Sato et al. (1996) and Berlemont et al. (1997) both have the similar tendency to yield the prediction of the gas isotropic turbulence, which is, however, against the experimental measurements. Similar observations can also be found for the three gas velocities shown in Fig. 3 for station $x = 250$ mm. Therefore, it can be concluded that the Reynolds-stress model has the advantage over the k–ε models in that the gas turbulence anisotropy can adequately be predicted. It has been found (Chen and Pereira, 1995) that the correct prediction of the fluid turbulence anisotropy is a prerequisite for the correct prediction of the particle dispersion in anisotropic turbulent carrier flows.

Now, the present particle dispersion model is evaluated for the particle-laden turbulent gas flow. The numerical results of Sato et al. (1996) and Berlemont et al. (1997) were based on the time-correlated particle dispersion model (Berlemont et al., 1990). A total of 33,000 trajectories were tracked in the Lagrangian computations of Sato et al. (1996). In addition, more than 20,000 particle trajectories were tracked for the numerical results of Berlemont et al. (1997). The two-way coupling sources were accounted for in the same way as the present work. The comparison of the present three numerical results (Runs 1–3) has demonstrated that, for the two-phase flow considered in this work, the particle flow predictions are not very sensitive either to the time and length scales or to the maximum interaction time $T_{\max}$. There are slight

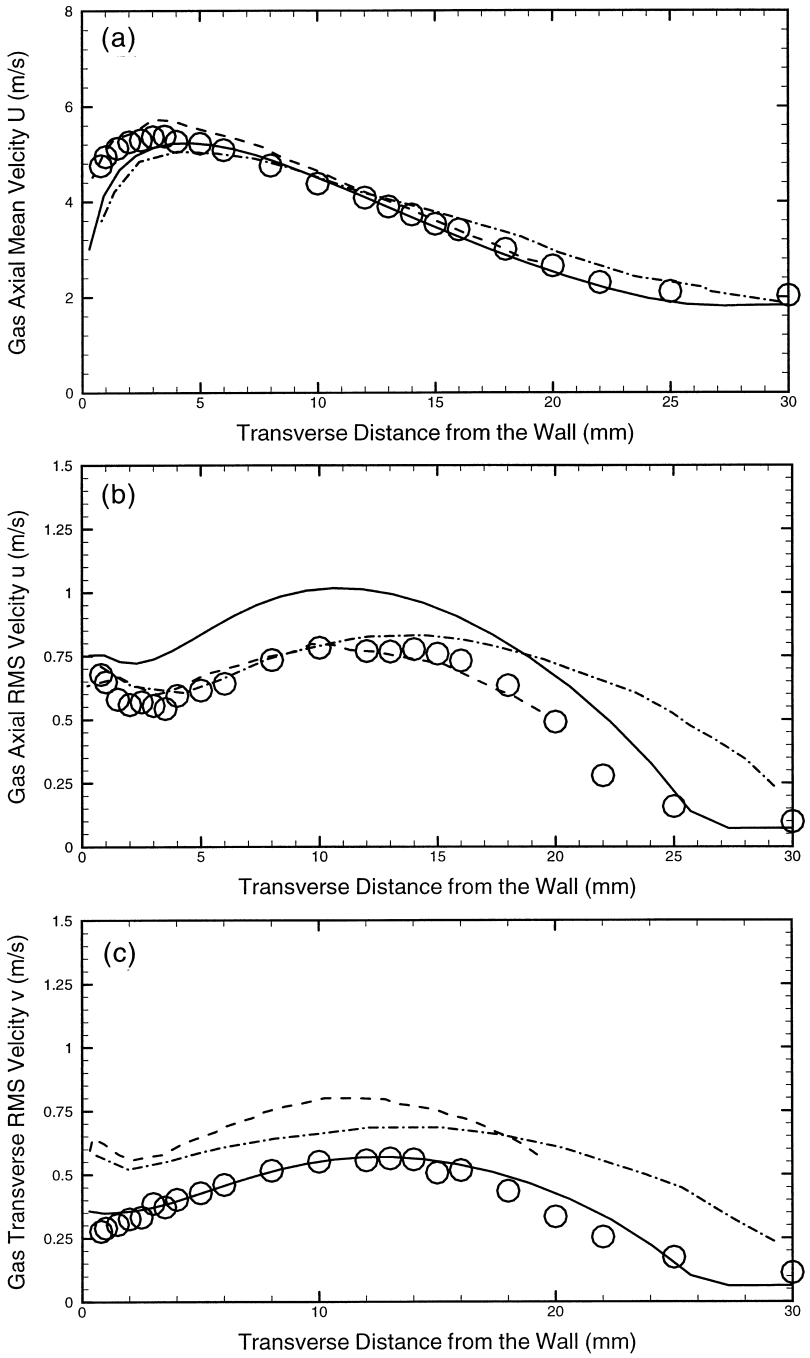

Fig. 2. Profiles of the single-phase flow: (a) axial mean, (b) axial RMS and (c) transverse RMS velocities at $x = 200$ mm. Keys: solid, predictions (present); dash, predictions (Sato et al., 1996); dash dot, predictions (Berlemont et al., 1997); symbols, data (Sato et al., 1996).

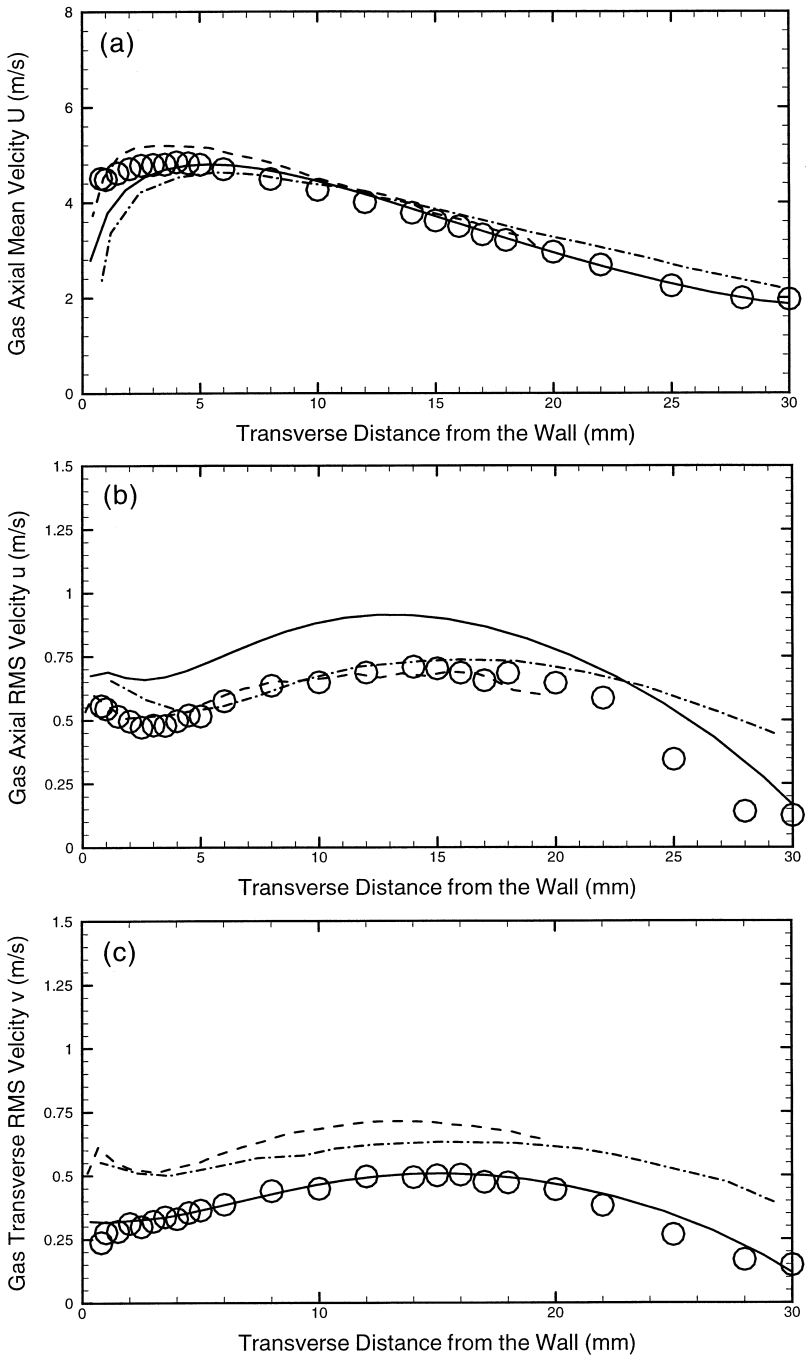

Fig. 3. Profiles of the single-phase flow: (a) axial mean, (b) axial RMS and (c) transverse RMS velocities at $x = 250$ mm. Keys are the same as those in Fig. 2(a)–(c).

discrepancies among the three numerical results. However, Run 3 can be regarded as a standard one which has accounted for the correct time and length scales and particle inertia (Graham, 1996a) in determining the particle-eddy interaction time. It is, therefore, considered for the following model evaluation.

Fig. 4(a)–(c) show the profiles of the particle and gas velocities at station $x = 200$ mm for the axial mean, axial and transverse fluctuating (RMS) values, respectively. The present numerical results (Run #3) are compared with both the numerical results and the experimental measurements of Sato et al. (1996). Moreover, some available numerical results (axial mean velocity) of Berlemont et al. (1997) are also shown in Fig. 4(a) for comparison. Unfortunately, their predictions of gas and particle fluctuating (RMS) velocities are not available. For the gas flow, Fig. 4(a) shows that the present Reynolds-stress transport model and the standard k–ε model of Berlemont et al. (1997) generally overpredict the gas axial mean velocity, whereas the predictions of Sato et al. (1996) using the low-Reynolds number k–ε model agree well with their measurements. The most probable reason for the discrepancy should arise from the two-way coupling sources, since the gas axial mean velocity has been well predicted with the Reynolds-stress model; see Figs. 2(a) and 3(a). For the particle flow, however, the present model predictions are generally in better agreement with the experimental measurements than the numerical results of Sato et al. (1996) and Berlemont et al. (1997). Even though the three models overpredict the particle axial mean velocity as a whole, the present particle dispersion model accounting for several additional physical phenomena still shows its superiority to the other two time-correlated particle dispersion models. Of interest is that the predictions of the gas axial mean velocity by Sato et al. (1996) agree satisfactorily with their experimental measurements, but their model much overpredicts the particle axial mean velocity. In contrast, the overprediction of the gas axial mean velocity by the present model is consistent with the overprediction of the particle axial mean velocity. Comparing the predictions for the clean air in Fig. 2(a) and for particle-laden air in Fig. 4(a), one can note that the particle-laden air mean velocity is smaller than the clean air value. This is because the particles lag behind the gas phase at the inlet. The two-phase momentum exchange leads to a loss of gas momentum, which turns to accelerate the particle phase. As a result, the gas axial mean velocity for the two-phase flow becomes smaller than it is for the single-phase flow.

The comparison of the particle fluctuating (RMS) velocities in Fig. 4(b) and (c) clearly indicates the particle turbulent property, especially the particle axial fluctuating velocity, is much better predicted with the present particle dispersion model that has taken into account several additional physical phenomena. In contrast, the numerical results of Sato et al. (1996) show much underprediction of the particle axial fluctuating velocity; see Fig. 4(b). Of particular note is that many zigzag changes are present in the numerical results of Sato et al. (1996), even though more particle trajectories (33,000) were tracked for their time-correlated particle dispersion model. Fig. 4 shows that an adequate account of different physical phenomena, such as turbulence inhomogeneity, turbulence anisotropy and particle inertia, for particle dispersion can reasonably well predict the particle turbulent property (the fluctuating velocity). For the gas flow, the axial fluctuating velocity is overpredicted with the Reynolds-stress model, but is satisfactorily predicted by the low-Reynolds number k–ε model of Sato et al. (1996). As mentioned before, an opposite performance of the two models can be observed for the gas transverse fluctuating velocity; a better prediction with the Reynolds-stress model.

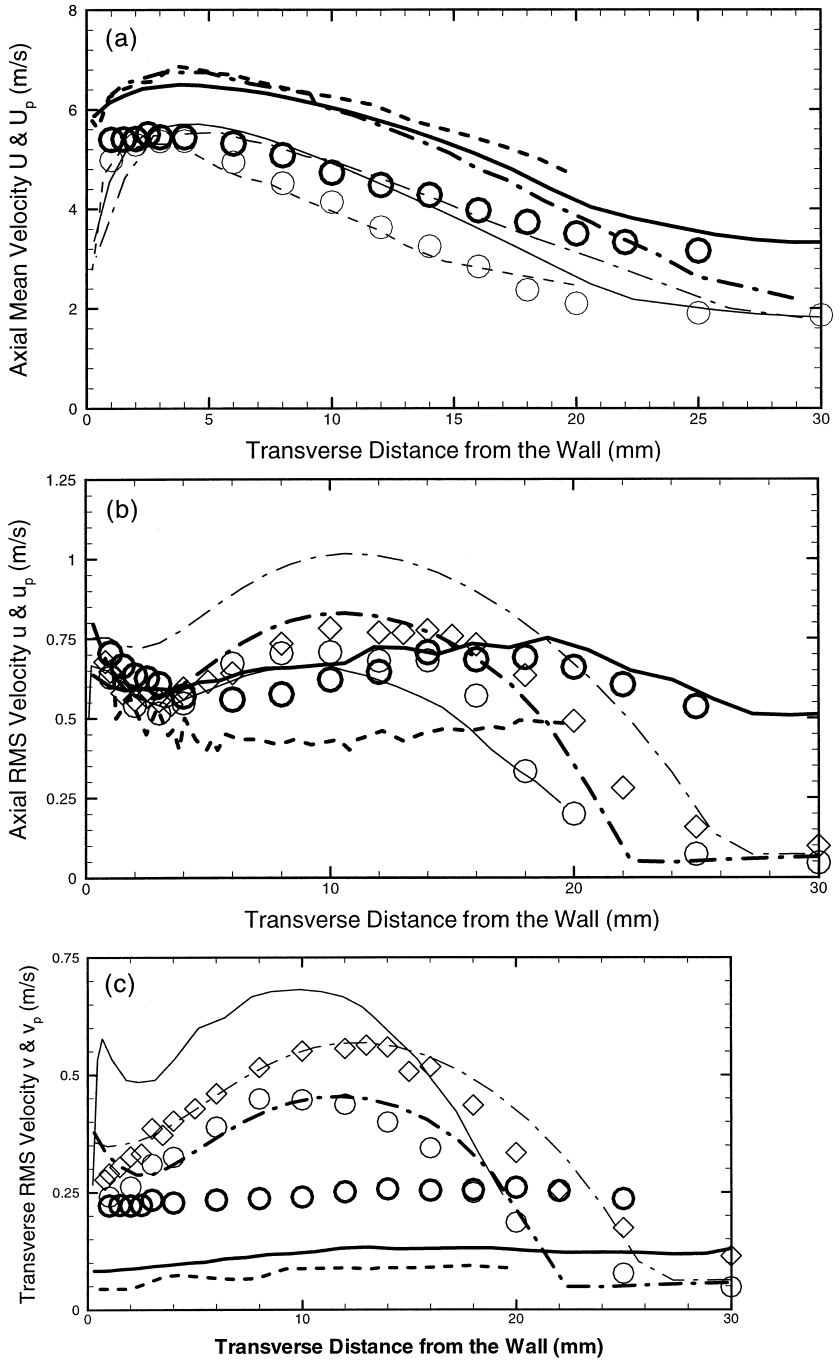

Fig. 4. Profiles of the two-phase flow: (a) axial mean velocity, (b) axial RMS and (c) transverse RMS velocities at $x = 200$ mm. Keys for (a): bold solid, particle predictions (present); bold dash, particle predictions (Sato et al., 1996); bold dash dot, predictions (Berlemont et al., 1997); bold circle, particle data (Sato et al., 1996); solid, particle-laden air predictions (present); dash, particle-laden air predictions (Sato et al., 1996); dash dot, particle-laden air predictions (Berlemont et al., 1997); circle, particle-laden air data (Sato et al., 1996). Keys for (b) and (c): bold solid, particle predictions (present); bold dash, particle predictions (Sato et al., 1996); bold circle, particle data (Sato et al., 1996); bold dash dot, particle-laden air predictions (present); solid, particle-laden air predictions (Sato et al., 1996); circle, particle-laden air data (Sato et al., 1996); dash dot, clean air predictions (present); diamond, clean air data (Sato et al., 1996).

However, the advantage of using the Reynolds-stress model is its ability to predict the anisotropy of gas turbulence. This can be clearly noted when comparing the gas axial fluctuating velocity with its transverse fluctuating velocity, as shown in Fig. 4(b) and (c). It is evident that the Reynolds-stress transport model has captured the turbulence anisotropy, yielding better predictions of the gas transverse fluctuating velocity. On the contrary, the low-Reynolds number k–ε model has much overpredicted the transverse fluctuating velocity, showing its incapability of capturing the turbulence anisotropy. The two components of the gas fluctuating velocity are almost isotropically predicted with the k–ε model, even though experiment indicates that the turbulence is still anisotropic. The same behavior can be observed for the three model results in Fig. 5 for station $x = 250$ mm. Figs. 4 and 5 have shown that the particle transverse fluctuating velocities are much underpredicted either by the present particle dispersion model or by the time-correlated dispersion model (Berlemont et al., 1990) as compared to the experimental measurements. As explained by Sato et al. (1996), the most probable reason for this large discrepancy between the predictions and measurements may arise from the high charge built up on the wall, which can significantly influence the motion of heavy nickel particles. However, the effect of wall charge on particle dispersion has not been accounted for in all numerical predictions. Even so, the present numerical results are still slightly superior to those of Sato et al. (1996).

The particle mean and fluctuating velocities are obtained using the ensemble averaging procedure for all the particle trajectories that cross the Eulerian control volume in question. However, the particle volume concentration is obtained using the *total* number of particle trajectories that cross the Eulerian control volume. Evidently, the volume concentration is a measure for the spatial distribution of physical particles in the computational domain. Fig. 6 show, respectively, the profiles of the particle volume concentration at station $x = 200$ and 250 mm. Once again, the present numerical predictions are compared with those of Sato et al. (1996) and Berlemont et al. (1997). Evidently, the present numerical predictions agree more satisfactorily with the measurements than either those of Sato et al. (1996) or those of Berlemont et al. (1997) for the region away from $y = 20$ mm. However, underprediction has been observed in the region close to the wall. This is the case for all the three model predictions. Experimental measurements indicate that more particles are distributed in the near-wall region, forming a high concentration profile there. Qualitatively, the present predictions and those of Berlemont et al. (1997) show the same tendency as the experiment, whereas the numerical predictions of Sato et al. (1996) clearly fail to correctly predict the distribution of physical particles, showing a high particle concentration around $y = 12$ mm. It is particularly noted that there appears a lot of computational noise in the concentration profiles of Sato et al. (1996), although more particles were tracked in their computations. Similarly, some zigzag changes are also present in the results of Berlemont et al. (1997), even though these zigzag changes are much milder than those of Sato et al. (1996). Among the three models, the smoothest and best predictions are obtained with the present particle dispersion model. The present smooth profiles are likely to benefit from the numerical algorithm used in the present work for distributing particle sources and assigning the particle property (Chen and Pereira, 1999) to the particle-crossed Eulerian control volumes in terms of the time-residence interpolation.

Several factors may be responsible for the high particle volume concentration in the near-

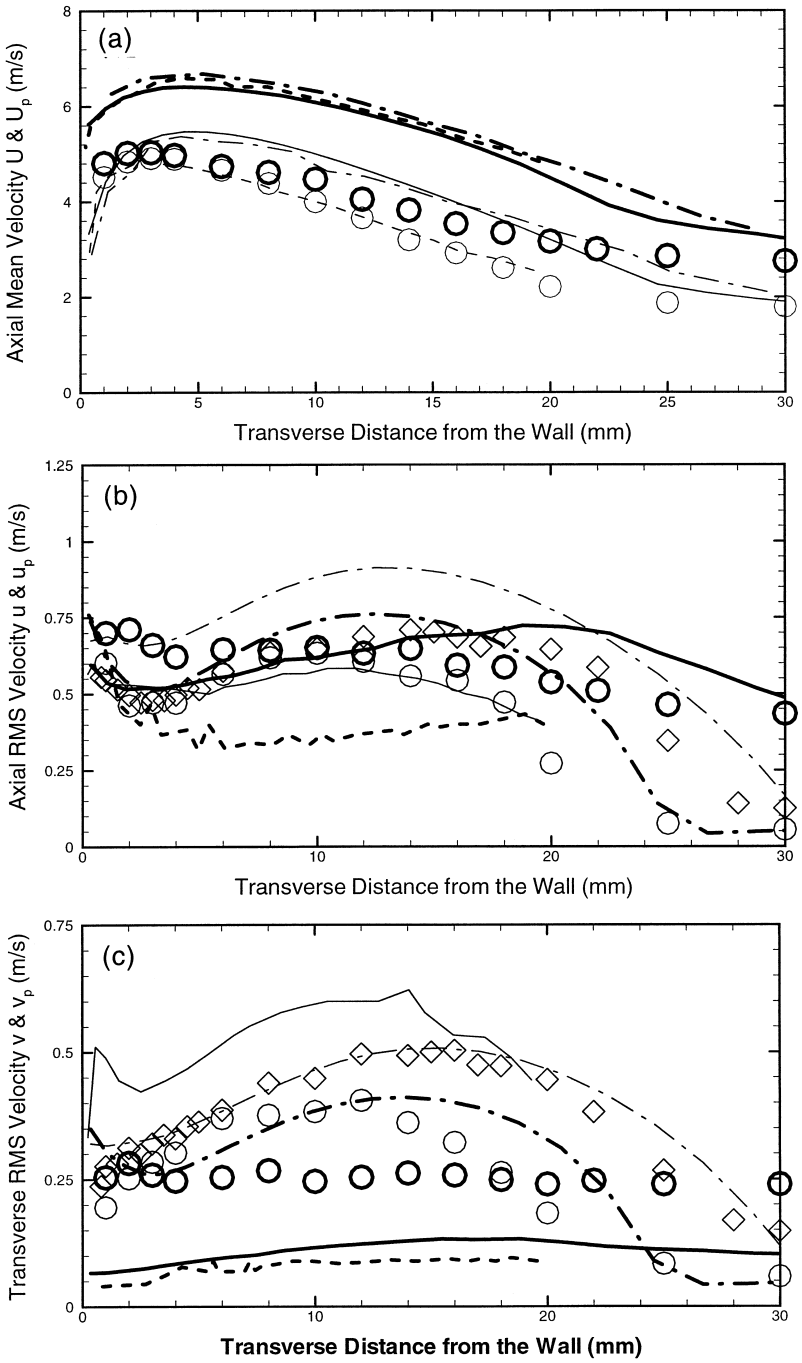

Fig. 5. Profiles of the two-phase flow: (a) axial mean, (b) axial RMS and (c) transverse RMS velocities at $x = 250$ mm. Keys for (a) are the same as those for Fig. 4(a) and keys for (b) and (c) are the same as those for Fig. 4(b) and (c).

wall region. It can be inferred that the high near-wall concentration may arise either from the particle migrating (transverse) velocity or from the particle-wall interactions (restitution coefficients), both of which should have a direct impact on the distribution of the predicted particle volume concentration. To clarify the effect of the migrating velocity on the particle volume concentration, numerical studies were carried out using different particle mean transverse velocities at the inlet; see the description for Runs 4–6 in Table 2.

7.2. Effect of initial conditions

The effect of the initial particle mean velocity on two-phase flow predictions was studied by changing the particle mean velocity at the inlet, corresponding to half and one-fourth of the experimental values (Runs 4–5) and zero (Run 6). Note that the particle fluctuating velocity was kept the same for all the three runs, as described in Table 2. Fig. 7(a)–(c) show, respectively, the profiles of the particle volume concentration, particle axial mean velocity, and

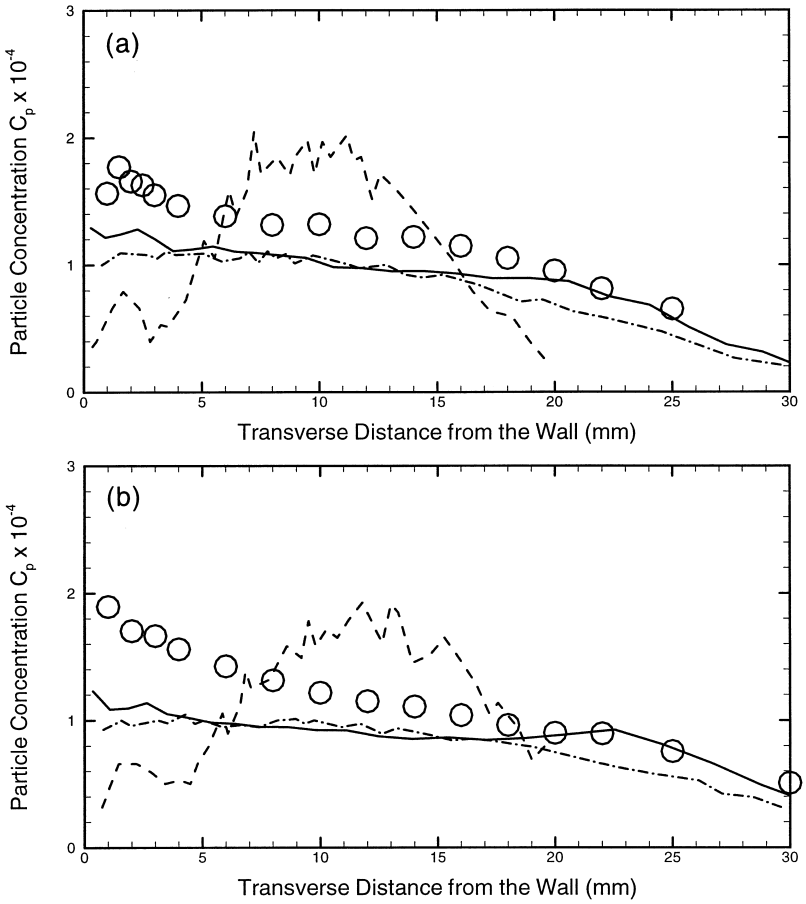

Fig. 6. Profiles of the particle volume concentration: (a) $x = 200$ mm and (b) $x = 250$ mm. Keys are the same as those in Figs. 2 and 3(a) and (b).

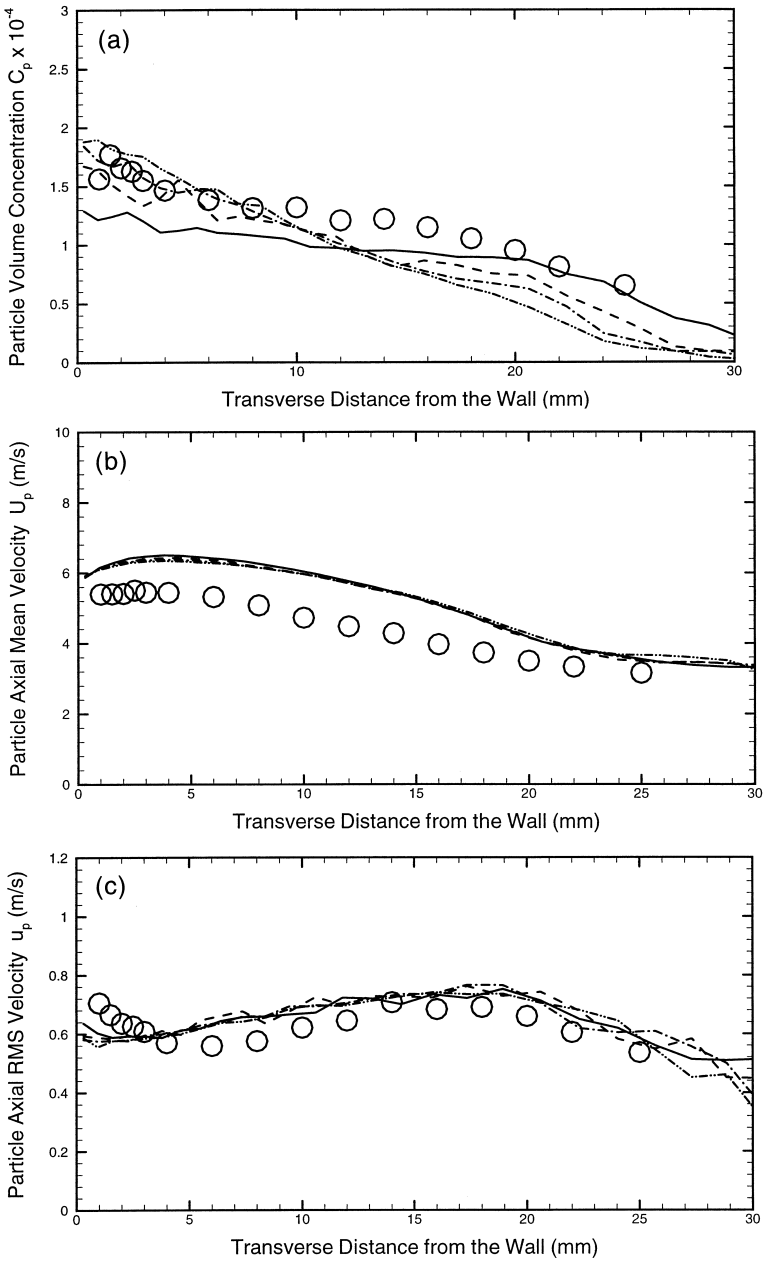

Fig. 7. Effect of initial conditions on predictions: (a) particle concentration, (b) particle axial mean and (c) axial RMS velocities at $x = 200$ mm. Keys: solid, Run 3; dash, Run 4; dash dot, Run 5; dash dot and dot, Run 6; circle, data (Sato et al., 1996).

particle axial fluctuating (RMS) velocity for the three runs at $x = 200$ mm. Note that Run 3 is also shown here for reference. As expected, the reduced particle mean velocity at the inlet results in reduced particle dispersion, thus increasing the particle volume concentration close to the wall; see Fig. 7(a). However, the improved agreement of the concentration with the experiment in the region close to the wall is at the expenses of reducing the particle dispersion. As a result, the concentration is underpredicted for the region away from the wall. Fig. 7(b) shows that the particle axial mean velocity is slightly sensitive to the change in the particle transverse mean velocity at the inlet. The reduced particle dispersion as a result of using the smaller transverse mean velocity at the inlet can also be observed in Fig. 7(c). The relatively larger discrepancy among the three runs occurs in the region farther away from the wall ($y >$ 20 mm), where the particle concentration is particularly sensitive to the particle mean velocity at the inlet. It should be noted that the zigzag changes in the region far away from the wall are due to the small number of particles present there, which increases the statistical uncertainty there. Similar observations have also been found for the profiles of the particle transverse fluctuating velocity; they are, therefore, not shown here. Of interest is that the near-wall gas fluctuating velocities are insensitive to the change in the initial particle mean velocity, showing almost no difference among the three runs.

7.3. *Effect of coupling sources*

So far, all the numerical predictions have accounted for both the two-phase momentum exchanges and the turbulence modulation of the gas phase by the dispersed particle phase; that is, the complete two-way coupling effect has been accounted for in two-phase flow predictions. To separate the influence of the momentum exchanges from that of turbulence modulation, Runs 10 and 11 were carried out that accounted for only momentum exchanges (the partial coupling) and no coupling, respectively. The corresponding results, together with those of Run 3, are compared with each other and with those of Sato et al. (1996) in Fig. 8(a)–(c) for the two-phase axial mean, axial fluctuating velocity, and transverse fluctuating velocity, respectively. The almost identical results between Run 3 and 10 show that the particle-phase predictions are mainly influenced by the momentum exchanges. Therefore, the turbulence modulation can be neglected, as far as the particle flow predictions are concerned. To our surprise, this is not the case for the fluid gas flow; see Fig. 8(a)–(c) for the gas flow predictions. Compared with the clean air predictions (Run 11), the particle-laden air predictions show that the fluid turbulence in the presence of nickel particles is generally attenuated as a result of the turbulence modulation. Fig. 8(b) and (c) show that the numerical predictions qualitatively agree with the measurements, i.e., to attenuate the fluid turbulence as compared to the clean flow. Such a turbulence-modulation phenomenon also agrees with the theoretic analysis (Gore and Crowe, 1989) that small particles attenuate the fluid turbulence. For the present two-phase flow, it was found that the maximum relative Reynolds number (Re_p) was less than 400. Therefore, the turbulence attenuation by the added particles also agrees with the theoretic analysis of Hetsroni (1989), who discriminated the turbulence attenuation and augmentation based upon the demarcating Reynolds number, $Re_p = 400$.

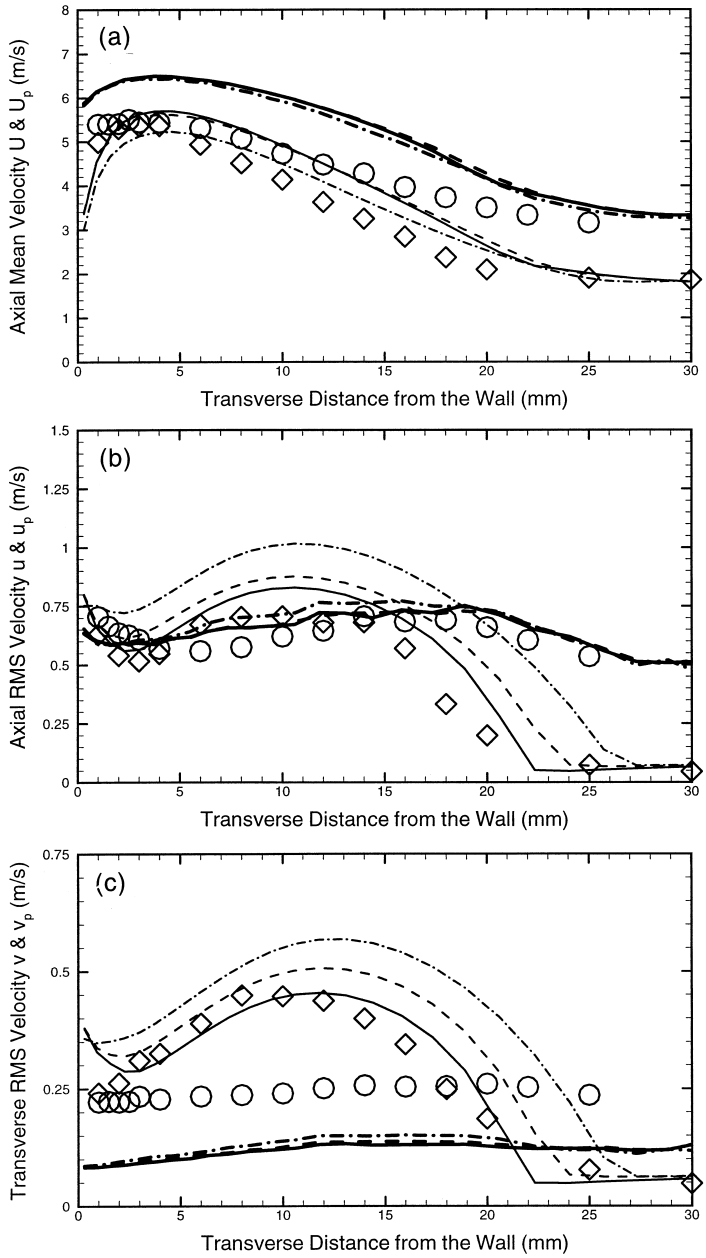

Fig. 8. Effect of coupling sources on predictions: (a) particle axial mean, (b) particle axial and (c) transverse RMS velocities at $x = 200$ mm. Keys: bold solid, particle predictions (Run 3); bold dash, particle predictions (Run 10); bold dash dot, particle predictions (Run 11); circle, particle data (Sato et al., 1996); solid, particle-laden air predictions (Run 3); dash, particle-laden air predictions (Run 10); dash dot, clean air predictions (Run 11); diamond, particle-laden air data (Sato et al., 1996).

7.4. Effect of restitution coefficients

As inferred before, the high near-wall particle volume concentration in the experiment may also arise from the particle-wall interaction. This is because particle-wall interaction causes the particle energy loss and reduces the particle migrating (transverse) velocity. To clarify how particle-wall interaction influences the two-phase flow predictions, the numerical predictions for Runs 3, and 7–9 are compared. These runs are different from each another in the restitution coefficients used to account for particle-wall interaction. For the two-phase flow considered here, it was found that the impact angles were very small owing to the prevalent axial mean velocity. As a result, the restitution coefficients (Jun and Tabakoff, 1994) are approximate to unity. The comparison of the results for these runs has shown that no discernible discrepancies are observed among the results. Therefore, they are not plotted here anymore. It can, thus, be concluded that the particle-wall interaction is not the factor responsible for the high particle volume concentration close to the wall.

7.5. Evaluation of model accuracy

So far all the numerical predictions have been compared with the experimental measurements using the transverse profiles. To have an idea of how these models are quantitatively compared with the measurements, numerical errors are estimated for the three model predictions for an arbitrary position in $x = 200$ mm and $y = 15$ mm, as suggested by one referee. Table 3 lists the detailed error estimations for the single-phase flow predictions. As shown in Figs. 3 and 4, the predictions of Sato et al. (1996) yield the best agreement with the measurements for the gas axial mean velocity. It is found, however, that the Reynolds-stress model best predicts the gas fluctuating velocities. Note that, under the assumption of correct experimental measurements, the positive errors represent an overprediction, and that the negative errors represent an underprediction.

Table 4 gives a detailed list of estimated errors for all numerical runs and those for Sato et al. (1996) and Berlemont et al. (1997). Generally speaking, there are large discrepancies between predictions and measurements for the chosen position. It should be noted that these estimated errors are solely based on an arbitrary single point. They cannot, therefore, represent the general trend of the numerical predictions. For example, the particle volume concentration, predicted by Sato et al. (1996), agrees by chance well with the measurements at the chosen point. However, the general trend of the particle volume concentration, shown in Fig. 6(a) and (b), clearly demonstrates that the overall predictions of Sato et al. (1996) are very different

Table 3
Error (%) estimation at $(x, y) = (200 \text{ mm}, 15 \text{ mm})$ for the single-phase flow

Variable	Present model	Sato et al. (1996)	Berlemont et al. (1997)
U	−4.4	−0.4	11.2
u	21.2	−6.4	7.1
v	0	35.1	23.1

Table 4
Error (%) estimation at $(x, y) = (200\ \text{mm}, 15\ \text{mm})$ for the two-phase flow

Flow variable	Present model											Sato et al. (1996)	Berlemont et al. (1997)
	1	2	3	4	5	6	7	8	9	10	11		
U	25.6	25.8	26.1	21.8	19.8	18.2	25.2	24.7	24.7	26.9	13.4	−4.6	32.8
u	16.7	18.3	19.3	27.4	31.1	33.7	18.2	18.4	18.4	28.2	51.1	−18.5	Unavailable
v	13.5	14.9	15.6	22.4	25.8	27.9	14.5	14.8	14.8	31.6	50.2	48.2	Unavailable
U_p	26.6	26.7	27.7	27.9	27.7	28.8	26.1	25.9	25.9	28.4	23.8	34.5	23.1
u_p	2.4	4.3	2.6	4.2	5.6	5.4	0.6	1.4	1.2	3.9	10.4	−33.2	Unavailable
v_p	−62.2	−57.9	−57.7	−56.2	−52.1	−51.1	−58.9	−59.1	−59.2	−55.2	−51.1	−65.2	Unavailable
C_p	−17.8	−19.2	−20.2	−29.5	−30.5	−33.0	−17.5	−21.5	−21.6	−21.7	−20.7	1.1	−22.6

from their experimental measurements. Table 4 shows that the particle mean and fluctuating velocities are better predicted with the present particle dispersion model than either Sato et al. (1996) or Berlemont et al. (1997). Taking into account the fact that the glass particles for the same flow configuration have been well predicted with the present numerical model (Chen and Pereira, 1998), the large discrepancies are very likely from the buildup of wall charge in the experimental measurements.

8. Concluding remarks

Detailed numerical studies have been carried out for heavy nickel particles dispersing in a turbulent gas flow. Various aspects influencing two-phase flow predictions were addressed. The second-moment Reynolds-stress transport model in curvilinear coordinates was applied to predict the carrier flow field. The improved particle dispersion model has taken into account the additional effect that the heavy particle has the possibility to disperse faster than the fluid particles (Graham, 1996a, 1996b). Numerical results were compared with experimental measurements and other model predictions. The present study has come to the following conclusions.

1. The anisotropy of the fluid turbulence is satisfactorily predicted with the Reynolds-stress model. In contrast, the two versions of the k–ε model yield almost isotropic predictions of turbulence.
2. The transverse particle velocity at the inlet has a great impact on the particle volume concentration. The change in the particle mean transverse velocity at the inlet can substantially improve the predictions of the near-wall particle concentration. Even though the reduced particle mean transverse velocity at the inlet does bring the predicted near-wall concentration to more agreement with experimental measurements, however, this was achieved at the expenses of artificially reducing the transverse particle dispersion. As a result, general underprediction is observed for particle volume concentrations far away from the wall jet.
3. It was found that the maximum interaction time ($T_{\max}$) is only important to the finite-inertia (glass) particles where the eddy interaction time is dependent on this time scale (Chen and Pereira, 1998). Otherwise, $T_{\max}$ has a negligible effect on particle flow predictions because the eddy interaction time is mainly dependent on the eddy transit time. This is the case for the present turbulent gas flow laden with nickel particles.
4. The change in restitution coefficients has a negligible influence on the particle volume concentration. The fully elastic rebounding conditions may be used to account for particle-wall interaction for simplification.
5. The turbulence modulation has a little impact on the turbulence of the nickel particles, but has a non-negligible effect on the turbulence of the fluid flow, even though the particle volume concentration is very low. As far as the particle flow predictions are concerned, the two-way coupling effect between the gas and particles is mainly due to the momentum exchanges. Owing to the large particle relaxation time, no discernible discrepancy has been observed in numerical predictions with and without turbulence modulation for the particle

volume concentration, particle mean and fluctuating velocities. Of particular note is that the complete two-way coupling sources (both momentum exchanges and turbulence modulation) have to be accounted for, as far as fluid flow (turbulence) predictions are concerned.

6. Compared with other particle flow predictions of Sato et al. (1996), and Berlemont et al. (1997), present numerical results for the particle flow agree more satisfactorily with experimental measurements.

Acknowledgements

The author gratefully appreciates the comments from the three referees for improving the original manuscript.

References

Berlemont, A., Desjonqueres, P., Gousbet, G., 1990. Particle Lagrangian simulation in turbulent flows. Int. J. Multiphase Flow 16, 19–34.

Berlemont, A., Desjonqueres, P., Cabot, M.S., 1997. Turbulence modification in a particle laden wall jet. ASME FEDSM97, Paper No. 3577.

Chang, K.-C., Wu, W.-J., 1994. Sensitivity study on Monte Carlo solution procedure of two-phase turbulent flows. Numeri. Heat Transfer, Part A 25, 223–244.

Chen, P.P., Crowe, C.T., 1984. On the Monte-Carlo method for modeling particle dispersion in turbulent gas–solid flows. ASME FED 10, 37–48.

Chen, X.-Q., Pereira, J.C.F., 1995. Prediction of evaporating spray in anisotropically turbulent gas flow. Numeri. Heat Transfer, Part A 27, 143–162.

Chen, X.-Q., Pereira, J.C.F., 1996. Computation of turbulent evaporating sprays with well-specified measurements: a sensitivity study on droplet properties. Int. J. Heat Mass Transfer 34, 441–454.

Chen, X.-Q., 1997. An efficient particle-tracking algorithm for two-phase flows in geometries using curvilinear coordinates. Numeri. Heat Transfer, Part A 31, 387–405.

Chen, X.-Q., Pereira, J.C.F., 1997. Computational modeling of dilute gas-particle flows in an ultrasonic gas flowmeter. Flow Meas. Instru. 8, 167–182.

Chen, X.-Q., Pereira, J.C.F., 1998. Computation of particle-laden turbulent gas flows using two dispersion models. AIAA J. 36, 539–546.

Chen, X.-Q., Pereira, J.C.F., 1999. A new particle-locating method accounting for source distribution and particle-field interpolation for hybrid modeling of strongly coupled two-phase flows in arbitrary coordinates. Numeri. Heat Transfer, Part B 35, 41–63.

Crowe, C.T., 1982. Review — numerical models for dilute gas-particle flows. J. Fluids Eng. 104, 297–303.

Crowe, C.T., Troutt, T.R., Chung, J.N., 1996. Numerical models for two-phase turbulent flows. Ann. Rev. Fluid Mech. 28, 17–43.

Durst, F., Milojevic, D., Schonung, B., 1984. Eulerian and Lagrangian prediction of particulate two-phase flows: a numerical study. App. Math. Modeling 8, 101–115.

Elghobashi, S., 1994. On predicting particle-laden turbulent flows. Appl. Sci. Research 52, 309–324.

Gavze, E., Shapiro, M., 1997. Particles in a shear flow near a solid wall: effect of nonsphericity on forces and velocities. Int. J. Multiphase Flow 23, 155–182.

Gibson, M.M., Launder, B.E., 1978. Ground effects on pressure fluctuations in the atmospheric boundary layer. J. Fluid Mech. 86, 491–511.

Gore, R.A., Crowe, C.T., 1989. Effect of particle size on modulating turbulent intensity. Int. J. Multiphase Flow 15, 279–285.

Gosman, A.D., Ioannides, E., 1981. Aspects of computer simulation of liquid-fuelled combustors. AIAA paper 81-0323.

Graham, D.I., 1996a. On the inertial effect in eddy interaction models. Int. J. Multiphase Flow 22, 177–184.

Graham, D.I., 1996b. An improved eddy interaction model for numerical simulation of turbulent particle dispersion. J. Fluids Eng. 118, 819–823.

Graham, D.I., James, P.W., 1996. Turbulent dispersion of particles using eddy interaction models. Int. J. Multiphase Flow 22, 157–175.

Hetsroni, G., 1989. Particles-turbulence interaction, Int. J. Multiphase Flow 15, 735–746.

Jun, Y.-D., Tabakoff, W., 1994. Numerical simulation of a dilute particulate flow over tube banks. J. Fluids Eng. 116, 770–777.

Kohnen, G., Sommerfeld, M., 1997. The effect of turbulence modeling on turbulence modification in two-phase flows using the Euler/Lagrange approach. In: Ninth Sym. Turbulent Shear Flows, Grenobe, France, 3–23.

Lien, F.S., Leschziner, M.A., 1994. Assessment of turbulence-transport models including nonlinear RNG eddy-viscosity formulation and second-moment closure for flow over a backward-facing step. Comput. Fluids 23, 983–1004.

Lien, F.S., Leschziner, M.A., 1996. Second-moment closure for three-dimensional turbulent flow around and within complex geometries. Comput. Fluids 25, 237–262.

MacInnes, J.M., Bracco, F.V., 1992. Stochastic particle dispersion and the tracer-particle limit. Phys. Fluids A 4, 2809–2824.

Rizk, M.A., Elghobashi, S.E., 1989. A two-equation turbulence model for dispersed dilute confined two-phase flow. Int. J. Multiphase Flow 15, 119–133.

Sato, Y., Hishida, K., Maeda, M., 1996. Effect of dispersed phase on modification of turbulent flow in a wall jet. J. Fluids Eng. 118, 307–315.

Shuen, J.-S., Solomon, A.S.P., Zhang, Q.-F., Faeth, G.M., 1985. Structure of particle-laden jets: measurements and predictions. AIAA J. 23, 396–404.

Sirignano, W.A., 1993. Fluid dynamics of sprays — 1992: freeman scholar lecture. J. Fluids Eng. 115, 345–378.

Solomon, A.S.P., Shuen, J.S., Zhang, Q.-F., Faeth, G.M., 1985. Structure of nonevaporating sprays — I. Initial conditions and mean properties. AIAA J. 23, 1548–1555.

Zhou, Q., Leschziner, M.A., 1991. A time-correlated stochastic model for particle dispersion in anisotropic turbulence. In: Eighth Turbulent Shear Flow Symp.